POLITECNICO DI TORINO
Repository ISTITUZIONALE

Solar-driven calcium looping system for carbon capture in cement plants: Process modelling and energy analysis

Original
Solar-driven calcium looping system for carbon capture in cement plants: Process modelling and energy analysis / Ferrario, D., Stendardo, S., Verda, V., Lanzini, A.. - In: JOURNAL OF CLEANER PRODUCTION. - ISSN 0959-6526. - ELETTRONICO. - 394(2023). [10.1016/j.jclepro.2023.136367]

Availability:
This version is available at: 11583/2975746 since: 2023-05-26T11:10:54Z

Publisher:
Elsevier

Published
DOI:10.1016/j.jclepro.2023.136367

Terms of use:

This article is made available under terms and conditions as specified in the corresponding bibliographic description in the repository

Publisher copyright

(Article begins on next page)

17 September 2026

Journal of Cleaner Production 394 (2023) 136367

Contents lists available at ScienceDirect

Journal of Cleaner Production

journal homepage: www.elsevier.com/locate/jclepro

Solar-driven calcium looping system for carbon capture in cement plants: Process modelling and energy analysis

Daniele Ferrario [a,*], Stefano Stendardo [b], Vittorio Verda [a], Andrea Lanzini [a]

[a] Energy Department, Politecnico di Torino – C.so Duca Degli Abruzzi 24, 10129, Torino, Italy
[b] Italian National Agency for New Technologies, Energy and the Environment, ENEA, 00123, Via Anguillarese 301, Rome, Italy

ARTICLE INFO

Handling Editor: Cecilia Maria Villas Bôas de Almeida

Keywords:
Cement production
Carbon capture
Calcium-looping
Concentrated solar
Industry decarbonization

ABSTRACT

The cement industry produces around 6–7% of the global anthropogenic CO_2 emissions. This sector, therefore, needs to be decarbonized to meet the international goals on greenhouse gas emissions. In a cement plant, however, around 60% of the CO_2 emissions are hard-to-abate because they come from the calcination of the raw materials. Carbon capture is thus needed to perform deep decarbonization of the cement production process. Among all the carbon capture technologies proposed in the literature, Calcium looping (CaL) is one of the most promising ones. This work analyses on novel solar-driven CaL process for carbon capture in a cement plant. In the system proposed, the energy required for the CO_2 sorbent regeneration is fully supplied by a heliostat field. The performances of the overall system were evaluated through detailed process modelling and energy analyses. Primary energy consumption and CO_2 emissions (sum of both direct process emissions and indirect emissions due to electricity consumption) were assessed considering different grid electricity mixes and integration levels (IL) between the carbon capture system and the clinker kiln. We estimate that the integration of a solar-driven CaL in a cement plant could be able to reduce over 90% of the plant CO_2 emissions. Furthermore, this solution could potentially decrease the plant fuel consumption thanks to the reuse of the exhausted sorbent in the production process. On the other hand, a large heliostat field will be required to feed energy to the CaL process. Both the carbon intensity of the grid electricity mix and the IL impact on the system energy and carbon balance, as shown by the obtained values for the specific primary energy consumption for CO_2 avoided (SPECCA) index. Obtained SPECCA indexes vary between a maximum of 2.17 MJ/kg_{CO2}, obtained for an IL of 20% and grid electricity produced entirely from renewables, and a minimum of 0.57 MJ/kg_{CO2}, estimated for an IL of 80% and grid electricity produced from state-of-the-art pulverized coal.

1. Introduction

Cement production is one of the most energy consuming and CO_2 emitting industry sectors worldwide. It accounts for 6–7% of global anthropogenic GHG emissions, around 1.4 Gt of CO_2 emissions per year (Carbone et al. 2022). Therefore, efficient decarbonization measures should be carried out to meet the international goals in global greenhouse gas emissions reduction.

Cement production comprises three main steps: (i) raw material extraction and preparation; (ii) clinker production; (iii) cement mixing and milling. Among those, the clinker production process is the most energy and carbon intensive step. The process raw material is a fine powder, called "raw meal", that consists mainly of calcium carbonate ($CaCO_3$) with the addition of oxides of Si, Fe, and Al. In the clinker production step, the raw meal is burned in a kiln (clinker kiln) reaching sintering temperature. The $CaCO_3$ contained in the material is calcined and reacts with SiO_2, Fe_2O_3 and Al_2O_3 forming clinker (the main constituent of cement). Cement is eventually obtained by milling the clinker together with gypsum and other additives.

One characteristic of the cement production, and in detail of the clinker production step, is that only around 40% of CO_2 emissions come from fuel combustion while the remaining 60% are associated with calcination processes and thus hard-to-abate (De Lena et al., 2017). The most common decarbonization measures include: (i) clinker and raw meal substitution with alternative materials; (ii) reducing of the clinker to cement ratio; (iii) fuel shifting from conventional fuel to less carbon intensive fuels; (iv) improvements in energy efficiency (Fennell et al., 2021). These techniques, however, are estimated to reduce the sector's CO_2 emissions by only 20–25% by 2050 (Hills et al., 2016). Carbon

* Corresponding author.
E-mail address: daniele.ferrario@polito.it (D. Ferrario).

https://doi.org/10.1016/j.jclepro.2023.136367
Received 3 October 2022; Received in revised form 31 January 2023; Accepted 6 February 2023
Available online 6 February 2023
0959-6526/© 2023 The Authors. Published by Elsevier Ltd. This is an open access article under the CC BY license (http://creativecommons.org/licenses/by/4.0/).

Notation

AC_{eq}	Equivalent avoided CO_2
ACR	Avoided-Captured CO_2 Ratio
BREF	Bat Reference document
CaL	Calcium Looping
CC	Carbon Capture
CCS	Carbon Capture and Storage
CCR	Carbon Capture Ratio
CC - CaL	Carbon capture system based on CaL
CSP	Concentrated Solar Power
CSP - CaL	Concentrated Solar Power with CaL thermochemical energy storage system
DNI	Direct Normal Irradiance
E_{carb}	Carbonator CO_2 capture efficiency
E_{eq}	Carbonator CO_2 capture efficiency at equilibrium conditions between CaO and CO_2
F_0	Molar flow of $CaCO_3$ makeup in the CaL system
F_{CO2}	Molar flow of CO_2 in the clinker flue gas
F_R	Molar flow of CaO entering the carbonator
IL	Integration level
SPECCA	Specific Primary Energy Consumption
S_{he}	Heliostat field size
T_{carb}	Carbonator temperature
TCES	Thermochemical Energy Storage system
X_{ave}	Average sorbent activity
e_{clk}	Specific clinker direct CO_2 emissions
$e_{clk,eq}$	Specific clinker total CO_2 emissions
p_{carb}	Carbonator pressure
$p_{CO2,eq}$	CO_2 partial pressure at equilibrium condition between CaO and CO_2
q_{clk}	Specific clinker primary energy consumption
sf_{he}	Heliostat field size factor, ratio between the field area and the minimum required area
η_{ref}	Heliostat reflectivity
η_{clc}	Heliostat clean factor
η_{fld}	Heliostat field efficiency
η_{inc}	Incidence factor
η_{CPC}	Parabolic concentrator efficiency
η_{cal}	Rotatory calciner efficiency

Capture and Storage (CCS) technologies need to be implemented to perform deep decarbonization of the cement industry sector (IEA, 2021), (Plaza et al., 2020). Post-combustion carbon capture and oxy-fuel combustion are the most promising because they can abate also the CO_2 produced from the raw meal calcination. Regarding post-combustion carbon capture technologies, they usually rely on absorption processes (e.g., amine-based processes), adsorption processes (e.g. Calcium Looping – CaL), or membrane separation (Gardarsdottir et al., 2019). The integration of amine scrubbing systems, a post-combustion carbon capture technique employing amine solvents, has been extensively analysed in the literature. This technology already reached commercial-scale for coal power plants applications (IEAGHG, 2015), and will soon reach this milestone also for cement industry applications (Carbone et al. 2022), (Plaza et al., 2020).

CaL, instead, is an adsorption process based on the reversible reaction between CaO and CO_2 usually employing two fluidized bed reactors: a carbonator and a calciner. CO_2 reacts with CaO forming $CaCO_3$ in the carbonator while in the calciner the $CaCO_3$ is decomposed into CaO and CO_2. One application of this process is as a carbon capture system using calcium oxide as a CO_2 sorbent (CC-CaL) where the energy necessary for sorbent regeneration is usually supplied with fossil fuel oxy-combustion taking place directly inside the calciner. Alternative systems with separated combustion and indirect calciner heat supply are also reported in literature (Jayarathna et al., 2017), (Abanades et al., 2005). CC-CaL is considered one of the most promising carbon capture techniques for decarbonization of power production and carbon-intensive industry. The integration of CC-CaL with cement production is particularly interesting as cement plants already possess the infrastructure necessary for solid materials handling (Carbone et al. 2022), (De Lena et al., 2017). Furthermore, the high temperatures reached in the CaL process allow the recovery of part of the chemical energy supplied at the calciner that can be converted into electric energy thus potentially reducing the cement plant grid electricity consumption. Part of the solid recirculating in the CC-CaL needs to be purged to guarantee an acceptable adsorption capacity of the CO_2 sorbent, which decreases with the number of carbonation and calcination cycles. However, this mineral, which consists mainly of CaO, can be used in the clinker production process in substitution of typical raw material, reducing the kiln CO_2 emissions related to calcination processes. The CC-CaL process is usually integrated in the clinker production process as an end-of-pipe system (Tail-End CaL) (De Lena et al., 2017), (Atsonios et al., 2015), (Cormos and Cormos, 2017), some authors also proposed a fully integrated system (Integrated CaL) where the CaL oxy-calciner replace the pre-calciner of the traditional plant, and the carbonator capture the CO_2 produced in the rotatory kiln (De Lena et al., 2019). CC-CaL was already demonstrated in several pilot projects (Chang et al., 2014), (Arias et al., 2017) and it recently reached TRL 7 (Carbone et al. 2022), (Jordal et al., 2017).

CaL was also studied as a Thermo-Chemical Energy Storage system (TCES) for integration in concentrated solar power plant (CSP-CaL) (Chacartegui et al., 2016), (Ortiz et al., 2019). In this system, a heliostat field supplies thermal energy to the calciner that is then stored in chemical form (CaO) and sensible form as compressed CO_2. The stored energy is then released by the carbonator and used for power production.

Some authors proposed innovative solar-driven CaL systems for carbon capture in a coal power plant. Here, the energy needed for sorbent regeneration is supplied totally or partially from a heliostat field (Zhang and Liu, 2014)– (Khosravi et al., 2022). Zhang et al. (Zhang and Liu, 2014) and Zhai et al. (2016) analysed a co-driven CaL system for carbon capture applications in coal power plants, where the energy needed at the calciner is supplied both by coal oxy-combustion and solar energy. In this configuration, coal is used during night-time and to integrate the energy supplied by the heliostat field when needed. Khosravi et al. (2022), instead, proposed a full solar-driven CaL system avoiding additional fuel consumption for CO_2 capture. In this configuration, the calciner works only during daytime and two solid reservoirs are needed to store CaO and $CaCO_3$ for night-time operation. To our best knowledge, no similar configurations were proposed for carbon capture applications in other industries other than power production from coal combustion.

Regarding cement production, Gonzalez et al. (Gonzalez and Flamant, 2014) and Moumin et al. (Moumin et al.) proposed a hybrid solar and coal co-driven clinker production process where a solar calciner is utilized in the raw meal calcination. The configurations they proposed, however, are able to abate the CO_2 emissions due only to coal combustion in the traditional pre-calciner, which Moumin estimated around 21% of the total.

The focus of this work is the application of a novel solar-driven CaL system for carbon capture in the cement production process. The system proposed and described is an end of pipe system able to abate the CO_2 emissions due both to coal consumption and calcination without comporting additional fossil fuel consumption. Furthermore, the reuse of the CaL purged sorbent in the production process reduces the amount of

$CaCO_3$ calcined in the clinker kiln, thereby reducing its coal consumption.

2. Process description and assumptions

The process proposed in this work, shown in Fig. 1, comprises the following sub-systems.

- Clinker kiln: the state-of-the-art process for clinker production as described in the European Best Available Techniques Reference (BREF) report for the manufacture of cement.
- Solar-driven calcium looping: CaL post-combustion carbon capture system driven by solar energy.
- Heliostat field: heliostat field that harvests the solar energy used for the regeneration of the CO_2 sorbent.
- Rankine cycle: power production cycle for the recovery and valorisation of the heat produced at the carbonator.
- CO_2 compression system: compression system that brings the captured CO_2 at the pressure needed for long distance network transportation.

2.1. State-of-the-art clinker kiln

The state-of-the-art clinker kiln, as described in the BREF report, comprises a preheater, a pre-calciner, a rotatory kiln and a clinker cooler (Schorcht et al., 2013). The main characteristics of the process and the compositions of the coal and the raw meal are reported in supplementary material. The raw meal is first sent to the preheater, where it is heated in a series of five vertical cyclones by contact with the hot kiln exhaust gas. The heated minerals are then fed to the pre-calciner, placed at the bottom of the preheater, where around 96.5% (Fidaros et al., 2007) of the limestone is calcined producing lime and CO_2. The obtained material is then burned in the rotatory kiln where it reaches sintering temperatures (around 1400 °C) (John, 2020). The calcination is completed, and the main components of the clinker are formed. CaO reacts with SiO_2, Al_2O_3, and Fe_2O_3 forming dicalcium silicate or belite (Ca_2SiO_4, or C_2S as in cement chemistry notation), tricalcium aluminate ($Ca_3Al_2O_6$, or C_3A), tetracalcium alumino-ferrite ($Ca_4Al_2Fe_2O_{10}$, or C_4AF), and tricalcium silicate or alite (Ca_3SiO_5, or C_3S) (De Lena et al., 2017).

In our calculations, small amounts of C_2S, C_3S, C_3A and C_4AF are assumed to form already in the pre-calciner coherently with the results published by De Lena et al. (De Lena et al., 2017). To meet the process' energy demand, required to drive the endothermic reactions and to heat the minerals coal is burned in the pre-calciner and the rotatory kiln (De Lena et al., 2017), (Schorcht et al., 2013) (coal composition is reported in supplementary material). The obtained hot clinker is finally cooled down using ambient air, which is then used as combustion air in the pre-calciner and rotatory kiln (Schorcht et al., 2013).

2.2. Solar-driven calcium looping

The CC-CaL process is characterized by a very high emission abatement potential. This system normally employs two fluidized-bed reactors: a carbonator and a calciner. In the carbonator, operating at approximately 650 °C, CO_2 reacts with CaO, here used as CO_2 sorbent, following the exothermic carbonation reaction described in R. 1.

$$CaO + CO_2 \rightleftharpoons CaCO_3 + \Delta H, \qquad \Delta H^0_{ref} = \pm 179 \frac{kJ}{mol} \qquad \text{R. 1}$$

The obtained $CaCO_3$ is then regenerated into CaO in a second reactor working at around 900–950 °C, called calciner, following the reverse endothermic reaction (calcination) releasing CO_2. The thermal energy needed to drive the calcination is usually provided by oxy-combustion of

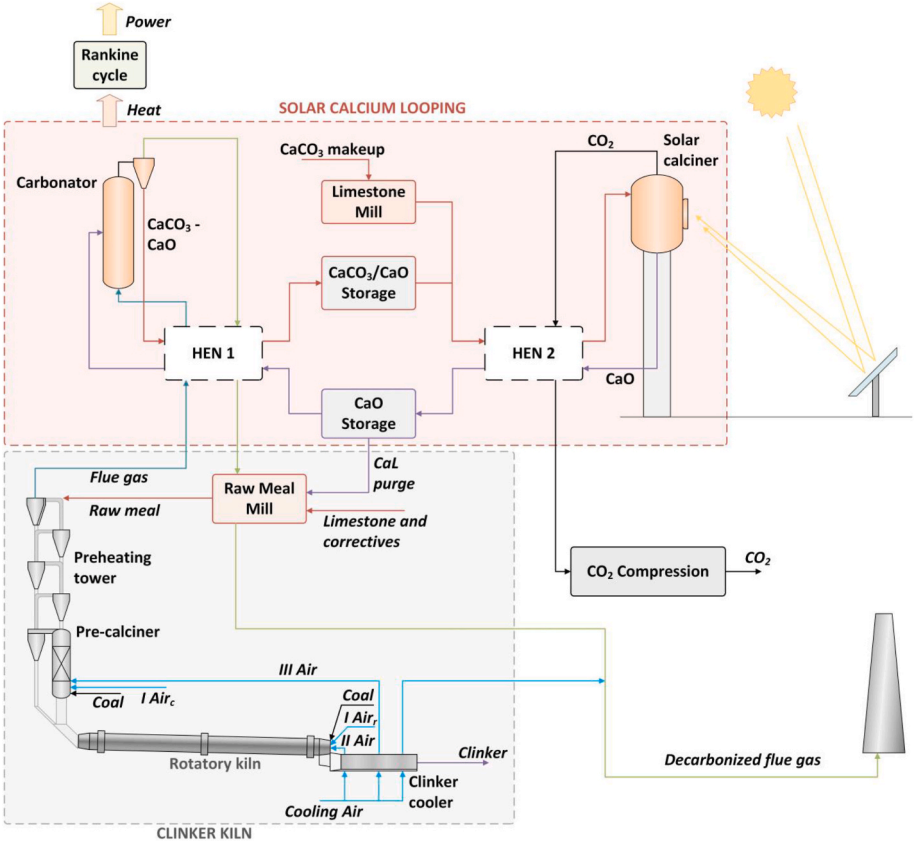

Fig. 1. Integration of a solar calcium looping in the cement production process.

traditional fossil fuels, carried out directly inside the calciner, producing high purity CO_2. An advantage of this technology is that, thanks to its high working temperature, part of the energy supplied to drive the CaL process can be recovered and easily converted into electricity with the aid of a traditional steam Rankine cycle (De Lena et al., 2017).

Regarding the application of CaL as thermochemical energy storage in CSP, solar energy coming from a heliostat field is utilized to drive the $CaCO_3$ calcination in a solar calciner. The released CO_2 is cooled, compressed, and sent to a pressurized storage tank, while the obtained CaO is cooled down to near ambient temperature and transported to a solids' reservoir. The solar energy is therefore stored in both sensible and chemical forms as compressed CO_2 and CaO. In the discharge phase, the CO_2 is first expanded in a turbine and then sent to the carbonator, where it is recombined with CaO, releasing heat, which is used for power production (Chacartegui et al., 2016). In this regard, different power cycles are proposed in the literature such as: closed CO_2 Brayton Cycles, supercritical CO_2 Brayton Cycles and steam Rankine cycles (Ortiz et al., 2019), (Ortiz et al., 2017). To maximize the energy storage efficiencies, two different heat exchanger networks (HENs) are placed before the carbonator (HEN1) and calciner (HEN2) to preheat the incoming streams while recovering heat from the outcoming flows (Ortiz et al., 2019).

The system configuration proposed and analysed in this work (Fig. 1) is a novel solar-driven CaL-based process for post combustion carbon capture in a cement plant. The system's main operating parameters assumed for the process modelling are summarized in Table 1. The flue gas exiting the clinker kiln is sent to the carbonator, where the CO_2 is captured by the solid sorbent (CaO). Before being released into the atmosphere, the CO_2 lean flue gas is cooled down to 430 °C and sent to the raw meal mill to provide the energy required for the raw meal drying (De Lena et al., 2017). The CO_2 rich sorbent, composed of $CaCO_3$ and unreacted CaO, is fed to a solid reservoir. To maximize the heat recoverable from the reactor, the incoming flue gas and CaO are preheated in the HEN1 using the hot outcoming solid and gas streams.

During daytime, the CO_2 rich sorbent is fed to the solar calciner where $CaCO_3$ is divided back into CaO and CO_2. The calciner working temperature is set at 920 °C (35–40 °C above equilibrium temperature) ensuring complete calcination (De Lena et al., 2017). The obtained CaO is sent to a second solid storage, while the CO_2 is sent to the compression unit. To minimize the amount of heat required in the calciner, the reactor's incoming solid stream is preheated in the HEN2 recovering heat from the outcoming CO_2 and CaO streams.

Considering the high temperature needed for calcination, a tower mounted solar receiver configuration is the most appropriate to be used. This kind of system can reach maximum temperatures of 1000 °C or over, depending on the type of receiver employed (Merchán et al., 2022). It should be noted that the efficiency of the solar plants is highly dependent on the receiver performance and that particle receiver technology, needed for solar CaL applications, is still under development (TRL 4–5) (Ortiz et al., 2021). In this regard, different technical solutions were proposed in the past such as: falling particle, centrifugal particle, fluidized bed and rotary kiln receivers (Ortiz et al., 2019), (Zsembinszki et al., 2018). Among those, solar calciners comprising a rotatory kiln receiver and a Compound Parabolic Concentrator (CPC) are the ones at the highest stage of development (Tesio et al., 2020).

The sorbent purged from the CaL process can be fed to the raw meal mill to partially replace the limestone supplied to the clinker kiln (Plaza et al., 2020). Because the average raw meal particle size is normally in the range of 10–20 μm, while the CaL carbonator operates with larger particle sizes of around 100–200 μm, the purge is milled before feeding to the production process.

The degree of integration between the carbon capture and the clinker production sections strongly influences on the overall system energy balance. In this work, we define the degree of integration through the Integration Level (IL) parameter, calculated as the ratio between the $CaCO_3$ fed to the CaL process and the total $CaCO_3$ consumed by the cement plant (Eq. (1)). At increasing IL values, the limestone that is calcined in the clinker production process decreases, thus reducing the kiln's coal consumption and CO_2 production. Different values of IL are considered: 20%, 40%, 60% and 80%.

$$IL = \frac{CaCO_3\ input\ to\ CaL}{CaCO_3\ input\ to\ the\ plant} \quad \text{Eq. 1}$$

The energy balance of the system described was obtained considering a carbonator CO_2 capture efficiency (E_{carb}), defined as the fraction of CO_2 removed from the flue gas in the carbonator, equal to 90%. E_{carb} can be obtained from the reactor mass balance as a function of the molar flows of CO_2 (F_{CO2}) and CaO (F_R) entering the carbonator.

$$E_{carb} = min\left(\frac{F_R X_{ave}}{F_{CO_2}}, E_{eq}\right) \quad \text{Eq. 2}$$

Where E_{eq} represents the carbonator CO_2 capture efficiency that can be potentially achieved when equilibrium conditions between CaO and CO_2 are reached and depends on the CO_2 equilibrium partial pressure ($p_{CO2,eq}$), which can be obtained from the carbonator operating pressure (p_{carb}) and temperature (T_{carb}) following Eq. (3) (Chacartegui et al., 2016). X_{ave}, instead, indicates the average fraction of active CaO reacting with CO_2 to form $CaCO_3$ that can be calculated as shown in Eq. (4) (Zhai et al., 2016), (Khosravi et al., 2022).

$$p_{CO2,eq} = 4.137 \bullet 10^7\ exp\left(-\frac{20474}{T_{carb}}\right) \quad \text{Eq. 3}$$

$$X_{ave} = \frac{f_m(1-f_w)F_0}{F_0 + F_R(1-f_m)} + f_w \quad \text{Eq. 4}$$

Where F_0 and F_R are the molar flow rate of the $CaCO_3$ make-up and the CaO entering the carbonator. The values for f_m and f_w empirical parameters are set to 0.77 and 0.17, as reported in literature for natural limestone and typical fluidized bed reactors' working conditions (Abanades et al., 2005), (Zhai et al., 2016), (Khosravi et al., 2022).

Table 1
Main assumptions for the CaL and the CO_2 compression.

Parameter	Value	Unit	Reference
Carbonator outlet temperature	650	°C	De Lena et al. (2017)
Calciner outlet temperature	920	°C	De Lena et al. (2017)
Pressure losses in carbonator, cyclones, and filters	20	kpa	De Lena et al. (2017)
Carbonator CO_2 capture efficiency - E_{carb}	90	%	De Lena et al. (2017)
Fans isoentropic efficiency	82	%	De Lena et al. (2017)
Cyclones' efficiency	99	%	Zhai et al. (2016)
Number of intercooled compression stages	5	n° stages	Posch and Haider (2012)
Intercooling temperature	25	°C	Posch and Haider (2012)
CO_2 compressors' isoentropic efficiency	75	%	Atsonios et al. (2015)
Compression delivery pressure	120	bar	Posch and Haider (2012)
HENs minimum temperature difference	15	°C	Tesio et al. (2020)

2.3. Heliostat field

The heliostat field is composed of many sun-tracking mirrors that concentrate the solar radiation to a tower-mounted receiver (that coincides with the solar calciner) providing the energy required for the decomposition of $CaCO_3$ (Khosravi et al., 2022), (Ortiz et al., 2018). The solar radiation collected by the heliostat field and hitting the receiver's

concentrator (Q_{rec}) can be estimated from the Direct Normal Irradiance (*DNI*) and the heliostat field area (S_{he}) as follows (Zhang and Liu, 2014), (Zhai et al., 2016):

$$Q_{rec} = \eta_{ref} \bullet \eta_{clc} \bullet \eta_{fld} \bullet \eta_{inc} \bullet DNI \bullet S_{he} \quad \text{Eq. 5}$$

Where η_{ref}, η_{clc}, η_{fld} and η_{inc} are reported in Table 2 and represent, respectively, the heliostat reflectivity, the heliostat clean factor, the heliostat field efficiency, and the incidence factor. Assuming a solar calciner composed of a rotatory kiln receiver and a CPC, the net amount of energy used in the calciner (Q_{cal}) can then be obtained from the concentrator efficiency (η_{CPC}) and the receiver' efficiency (η_{cal}) (Tesio et al., 2020).

$$Q_{cal} = \eta_{CPC} \bullet \eta_{cal} \bullet Q_{rec} \quad \text{Eq. 6}$$

The rotatory kiln receiver technology was recently tested at the pilot scale by Wu et al. (Wu, Trebing, Amsbeck, Buck, Pitz-Paal) who obtained a η_{cal} value of around 75% for an outlet solids' temperature of 900 °C, the same efficiency value was then assumed in this work. Furthermore, according to the literature (Tesio et al., 2020), the minimum operating thermal power of this type of calciner corresponds to 20% of the nominal power. It should also be noted that this component maximum size was reported to be 55 MW (Tesio et al., 2020), therefore, multiple calciners in parallel will be needed.

2.4. Power production cycle

The thermal energy produced in the carbonator side of the system is recovered to produce electricity in a steam Rankine power cycle. This technology is the commercial standard for CSP power plants (Liu et al.) and it was often proposed for both CC-CaL and CSP-CaL applications (De Lena et al., 2019), (Ortiz et al., 2017).

Fig. 2 shows a schematic of the power production cycle considered in this work, i.e., a reheat steam Rankine cycle with regeneration in three pre-heaters. A series of steam extractions are performed in the high- and low-pressure steam turbines and fed to the three pre-heaters: two countercurrent heat exchangers (R1-2) and one total mixer exchanger type (DEA). An additional low temperature economizer is placed after the low-pressure pump to permit the efficient recovery of the sensible heat contained in the solid sorbent exiting the carbonator. The Rankine main operational parameters, reported in Table 3, were chosen from data suggested by Ortiz et al. (2017) for CSP-CaL applications. Turbine and pump efficiencies were set to 0.9, and a exchangers minimum temperature difference of 10 °C was considered. A 1% pressure drop was assumed in all heat exchangers apart from the steam generator evaporator where it was considered negligible (see Table 3).

3. Methods

The mass and energy balances were solved with the aid of the process simulator Aspen Plus v10.0, where the CaL solar calciner was modelled in its average working condition (average power and mass flows). For the clinker kiln, and the Calcium Looping section, the Peng Robinson equation of state was used, while for the Rankine cycle the IAPWS formulation 1995 (IAPWS-95) was selected. The main system process units, rotary kiln, CaL system, Rankine cycle, and CO_2 compressors were represented with one or more Aspen Plus blocks. The reactions taking place in the production and carbon capture processes were modelled with standard models based on the minimization of Gibbs free energy when possible, otherwise fixed reaction rates were assumed as reported in Table 1 and Table S1 in supplementary material.

The minimum required heliostat field size ($S_{he,min}$) was then estimated considering a constant solar calciner energy consumption (MJ_{th}/kg_{CaO}), seasonal solids storage and site hourly irradiation data. The DNI data were obtained from the open access tool PVGIS (PVGIS, 2019) and represent the typical meteorological year for the Augusta cement production plant located in Sicily, Italy. Fig. 3 shows the corresponding daily irradiation (kWh/m^2). This region was already selected in past CSP projects. In 2010, for example, the "Archimede" CSP plant was inaugurated near Syracuse in Sicily (Enel, 2010).

It should be noted that a heliostat field with a dimension equal to $S_{he,min}$ will require a very large solid storage that may be difficult to realize. However, the dimensions of the storage could be reduced by oversizing the heliostat field. This will result in a large excess of heat during summer, but a lower deficit of CaO production during winter and a lower requirement for CaO long time storage. A sensitivity analysis was then performed to investigate the size of the CaO solid storage at different values of the heliostat field factor (sf_{he}), defined as the ratio between the actual size of the heliostat field (S_{he}) and $S_{he,min}$ ($sf_{he} = S_{he}/S_{he,min}$).

3.1. Thermal integration

Optimizing the heat recovery from an integrated industrial process such as the one under investigation is crucial to achieve high energy and environmental performances. In the analysed system gas-gas, gas-solid and solid-solid heat exchangers will be needed. To avoid direct contact between CaO and CO_2, which could lead to undesired sorbent carbonation, innovative indirect gas-solid heat exchangers should be employed (Ortiz et al., 2017). In this regards different solutions were proposed in the literature such as: heat transfer plates, shell-tubes and moving packed-bed based heat exchangers (Chacartegui et al., 2016), (Ortiz et al., 2019), (Jordison et al., 2007). The solid-solid heat exchangers could then be realised by coupling two solid-fluid indirect heat exchangers (Chacartegui et al. (2016) proposed using two heat transfer plates exchangers) with an intermediate heat-transfer fluid that is recirculated within the two sides.

Two HENs (see Fig. 4 and Table 4), i.e. one for the system carbonator side and one for the calciner side, were designed applying the pinch analysis method with the aid of package Aspen Energy Analyser v10.0, considering a minimum temperature difference of 15 °C. On the carbonator side, the flue gas and the CaO entering the reactor will need to be pre-heated, to maximize the heat available for power production. However, thermal energy can be recovered from the decarbonized gas and the carbonated sorbent. The decarbonized gas can be cooled down to 430 °C before being sent to the raw meal mill, while the carbonated sorbent needs to be cooled to near ambient temperature before being sent to the solid storage. Likewise, on the calciner side, the sorbent should be preheated before entering the reactor to minimize heat

Table 2
Main assumptions for the heliostat field and solar calciner.

Parameter	Symbol	Value	Unit	Reference
Heliostat reflectivity	η_{ref}	93	%	(Zhang and Liu, 2014), (Zhai et al., 2016)
Heliostat clean factor	η_{clc}	95	%	(Zhang and Liu, 2014), (Zhai et al., 2016)
Heliostat fields efficiency	η_{fld}	76	%	(Zhang and Liu, 2014), (Zhai et al., 2016)
Incidence factor	η_{inc}	99	%	(Zhang and Liu, 2014), (Zhai et al., 2016)
Parabolic concentrator efficiency	η_{CPC}	97	%	(Tesio et al., 2020), (Wu, Trebing, Amsbeck, Buck, Pitz-Paal)
Rotatory kiln receiver efficiency	η_{cal}	75	%	Tesio et al. (2020)
Calciner cut in power	–	20	%	Tesio et al. (2020)

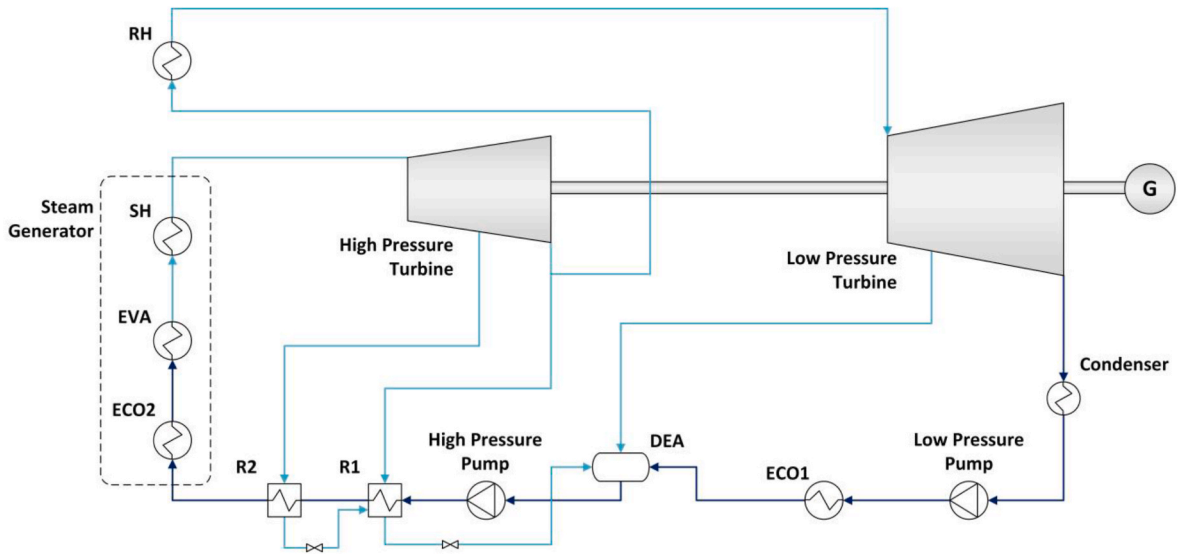

Fig. 2. Rankine cycle for power production.

Table 3
– *Assumption for the Steam Rankine cycle* (Ortiz et al., 2017).

Parameter	Value	Unit
HP turbine inlet pressure	160	bar
HP inlet temperature	540	°C
LP turbine inlet pressure	45.5	bar
LP turbine inlet temperature	540	°C
Condensation pressure	0.09	bar
HP and LP turbine isoentropic efficiency - η_t	0.9	–
HP and LP pump efficiency - η_p	0.9	–
Heat exchangers' pressure drop	1%	%
Heat exchangers' minimum temperature difference	10	°C

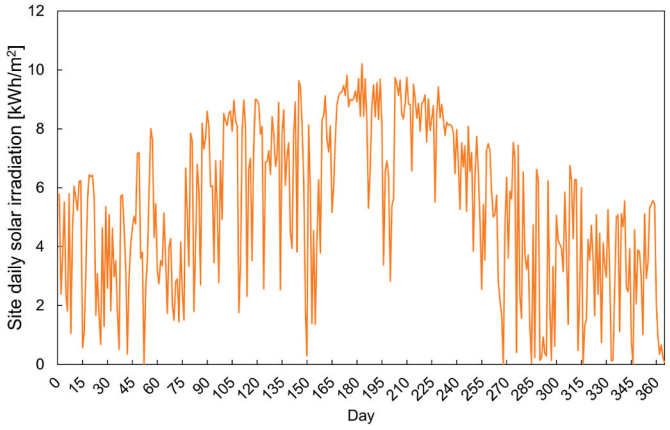

Fig. 3. Daily irradiance [kWh/m^2] for the selected site.

consumption. On the other hand, the hot CO_2 and the calcined sorbent need to be cooled down before being sent to the CO_2 compression and the solid storage.

3.2. Key performance indicators

The energy performances of the system were evaluated through the calculation of some Key Performance Parameters (KPIs), which are defined as follows.

- Specific primary energy consumption - q_{clk} [MJ/t_{clk}]:

$$q_{clk} = q_{fuel,clk} + q_{el,clk} + q_{sol,clk} \quad \text{Eq. 8}$$

Where $q_{fuel,clk}$ [MJ_{LHV}/t_{clk}] represents the primary energy consumption for fuel combustion; $q_{el,clk}$ [MJ_{LHV}/t_{clk}] is the net primary energy consumption due to the electricity exchanged with the grid; and $q_{sol,clk}$ [MJ_{th}/t_{clk}] is the solar contribution. The term $q_{el,clk}$ is obtained from the specific power consumption $P_{el,clk}$ [MJ_{el}/t_{clk}] and the electric generation efficiency of the electricity mix considered η_{el} [%], $q_{el,clk} = \frac{P_{el,clk}}{\eta_{el}}$. The value of $q_{sol,clk}$ was calculated using the "physical energy content method" (EUROSTAT, 2022) that in case of solar thermal assumes the primary energy consumption equal to the useful thermal energy produced by the solar plant.

- Specific CO_2 emissions - $e_{clk,eq}$ [kg_{CO2}/t_{clk}]: defined as the sum of direct emissions coming from combustion and calcination in the clinker kiln e_{clk} [kg_{CO2}/t_{clk}] and the indirect emissions due to electric energy consumption $e_{el,clk}$, estimated through the CO_2 emission factor for electric generation associated to the electricity mix considered, e_{el}.

$$e_{clk,eq} = e_{clk} + P_{el,clk} \bullet e_{el} \quad \text{Eq. 9}$$

Table 5 reports the electric generation efficiencies and CO_2 emission factors used. Four possible scenarios were considered: reference scenario, referred to the Italian 2019 electricity mix; scenario 1, electric production from a state-of-the-art coal power plant (same fuel as traditional cement plants); scenario 2, generation efficiency and CO_2 emission factor typical of the Italian thermoelectric power plants; and scenario 3, electricity generation from renewable sources.

- Carbon Capture Ratio - CCR [%]: ratio between the amount of captured CO_2, $m_{CO2,capt}$ [kg_{CO2}/t_{clk}], and the total amount of CO_2 generated by the plant, $m_{CO2,gen}$ [kg_{CO2}/t_{clk}].

$$CCR = \frac{m_{CO_2,capt}}{m_{CO_2,gen}} \quad \text{Eq. 10}$$

- Equivalent Avoided CO_2 - AC_{eq} [%]: the total avoided CO_2, considering both direct emissions and indirect emissions from electricity consumption.

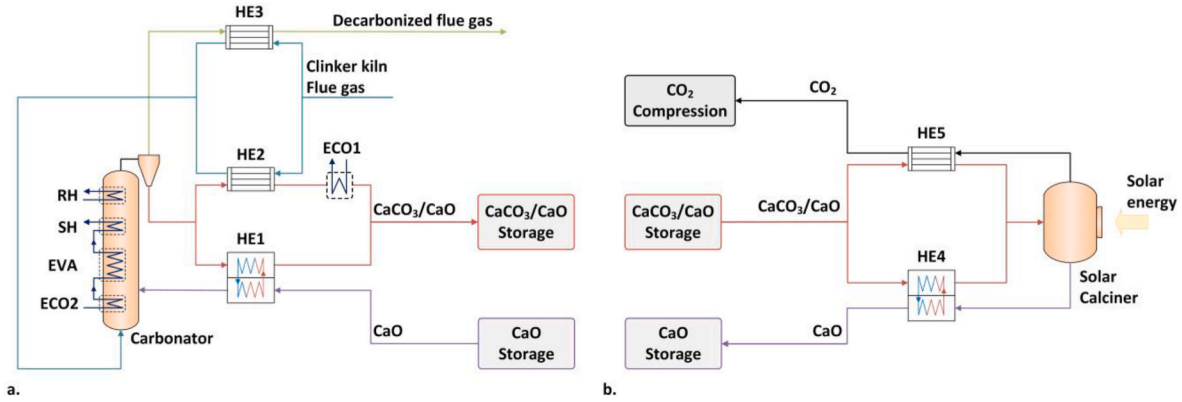

Fig. 4. Heat exchanger network for the carbonator side (a) and the calciner side (b).

Table 4
Details of the heat exchanger networks for IL 20%: heat exchangers type, size, and logarithmic mean temperature difference (LMTD).

Heat exchanger	Type	Size [MW_{th}]	LMTD [°C]
HEN1 - Carbonator side			
HE1	solid-solid	53.4	15
HE2	gas-solid	5.8	17
HE3	gas-gas	10.0	20
HEN2 - Calciner side			
HE4	solid-solid	80.4	23
HE5	gas-solid	25.9	37

Table 5
– Electric generation efficiencies and CO_2 emission factor for the generation mixes considered. Renewable energy sources' contribution was estimated through the "physical energy content method" (EUROSTAT, 2022).

Scenario	Electricity mix	Electric efficiency η_{el} [%]	CO_2 emission factor e_{el} [g_{CO2}/kWh]	Reference
Ref. Scenario	Italian electricity mix (2019)	53.0	277.3	ISPRA (2020)
Scenario 1	100% state-of-the-art pulverized coal	44.2	770.0	CEMCAP (2017)
Scenario 2	Average of Italian thermoelectric power plants (2019)	45.5	415.5	ISPRA (2020)
Scenario 3	100% Renewables	100	0	CEMCAP (2017)

$$AC_{eq} = \frac{e_{clk,eq,ref} - e_{clk,eq}}{e_{clk,eq,ref}} \quad \text{Eq. 11}$$

Where $e_{clk,eq,ref}$ is the equivalent CO_2 emissions for the reference non decarbonized clinker kiln and $e_{clk,eq}$ is the equivalent CO_2 emissions for the production plant integrated with the carbon capture system.

- Avoided-Captured CO_2 Ratio - ACR [-]: ratio between the effective amount of total avoided CO_2 and the respective amount of captured CO_2.

$$ACR = \frac{e_{clk,eq,ref} - e_{clk,eq}}{m_{CO_2,capt}} \quad \text{Eq. 12}$$

- Specific Primary Energy Consumption for CO_2 Avoided – SPECCA [MJ/kg_{CO2}]: represents the primary energy consumed to avoid the emissions of a mass unit of CO_2 in the atmosphere. It is defined as the ratio between the increase in the plant's primary energy consumption of the production and the amount of avoided CO_2.

$$SPECCA = \frac{q_{clk} - q_{clk,ref}}{e_{clk,eq,ref} - e_{clk,eq}} \quad \text{Eq. 13}$$

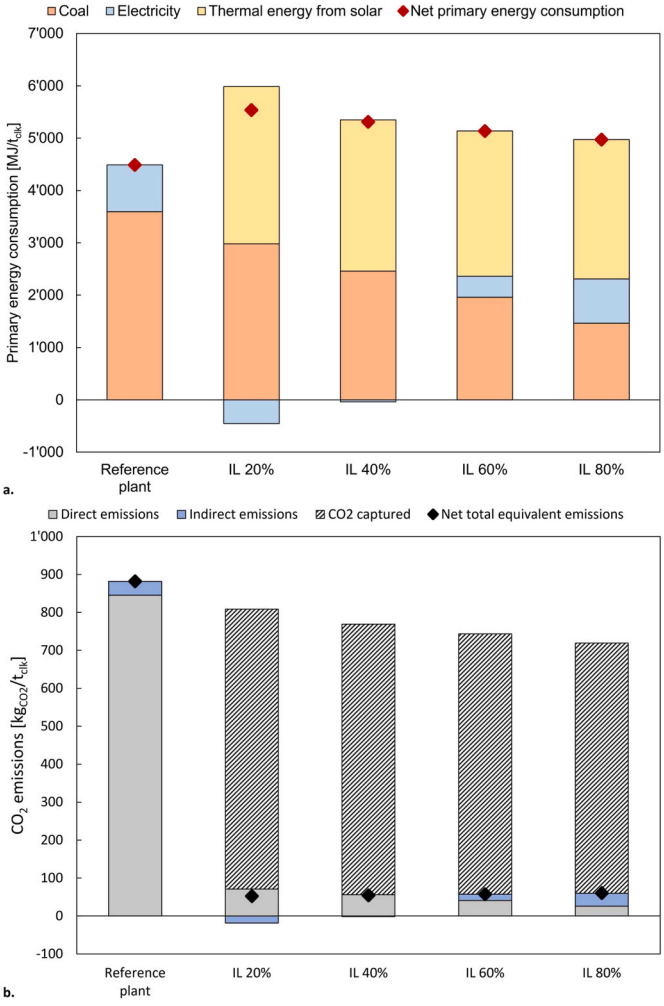

Fig. 5. Primary energy consumption and total CO_2 emissions for the reference production plant without carbon capture and the decarbonized system at different Integration Levels. Indirect CO_2 emissions and primary energy consumptions are estimated considering the Italian grid electricity mix.

4. Results and discussion

4.1. Performance of the analysed system configurations

Fig. 5 and Table 6 show the specific primary energy consumption, CO_2 emission and the detailed energy and mass balances for the reference plant and the solar CaL integrated system considering different integration levels. In our calculations, the Italian grid electricity mix (reference year 2019) was taken as the reference scenario. This mix is characterized by around 67% thermoelectric, 16% hydroelectric, 15% wind and solar and 2% of geothermal generation (ISPRA, 2020). The integration of solar CaL in the traditional clinker kiln allows a deep decarbonization of the system reducing the total CO_2 emissions from 882 kg_{CO2}/t_{clk} (reference kiln) to 60-52 kg_{CO2}/t_{clk} (solar CaL IL 20%–80%), corresponding to values of AC_{eq} of 94.1–93.2%. These latter high values, higher than the carbonator efficiency (90%), are a characteristic of CaL carbon capture systems. They are a consequence of the reuse of the purged CO_2 sorbent in the production process and the on-site electricity production from the Rankine cycle. The purged CO_2 sorbent, indeed, is composed of CaO produced at the solar calciner where the CO_2 from the calcination process is completely captured. This is reflected in the CCR indexes that reach values of 91.2%–96.2% (IL 20%–80%). Furthermore, the on-site power production reduces the amount of electricity absorbed from the grid, decreasing the indirect CO_2 emissions. In this regard, for low values of IL, the amount of electricity produced is greater than the plant's electricity consumption. The electricity surplus can therefore be exported to the grid, resulting in negative net indirect emissions. On the contrary, at high values of IL, the electricity production from the Rankine Cycle is not enough to cover all the electricity consumption, and power still needs to be imported from the grid.

Primary energy consumption, on the other hand, increases from 4′488 MJ/t_{clk} (reference clinker kiln) to 5′535–4′973 MJ/t_{clk} (IL 20%–80%) due to the additional thermal energy need of the solar calciner, resulting in SPECCA values of around 1.25–0.59 (IL 20%–80%). It should be noted that the convention used for the primary energy calculation associated with the solar energy consumption does not consider any conversion losses of the solar plant.

The supply of coal, which amounts to around 80% of the primary energy consumption of the reference plant for an IL of 20%, decreases with the integration of the solar CaL and it is further reduced at increasing values of IL. The CaO, purged from the carbon capture system and reused in the production process, indeed, is produced using renewable energy, decreasing the amount of coal necessary for raw meal calcination. At IL equal to 80% the fuel consumption amount to 1′465 MJ_{LHV}/t_{clk}, 41% of the reference plant consumption.

For the same reasons, the amount of CO_2 produced from combustion processes decreases in the solar CaL integrated configurations. This results in amounts of avoided CO_2 greater than the amounts of captured CO_2 and values of ACR higher than one around 1.13–1.25 (IL 20%–80%). In typical CC-CaL systems, instead, the regeneration of the solid sorbent is carried out with oxy-combustion of coal, resulting in amounts of avoided CO_2 lower than the amounts of captured CO_2 and ACR values lower than one: values of ACR around 0.6 can be estimated from data reported in the literature (De Lena et al., 2017). Therefore, lower energy consumption for CO_2 compression, transportation and storage should be expected for solar-driven CaL systems with respect to typical CC-CaL systems.

A sizing of the heliostat field was also performed. The estimated field area necessary to provide the required thermal energy to the solar calciner is around, 0.94–0.83 km^2 (IL 20%–80%), slightly larger sizes are estimated for low IL values. At high IL values, indeed, the CO_2 produced at the clinker kiln is reduced, and at the same time higher values of X_{ave} are reached, which reduce the amount of solid looping in

Table 6
Plant mass and energy balance and KPIs for different IL. Indirect CO_2 emissions and primary energy consumptions are estimated considering the Italian grid electricity mix.

Parameter	Symbol	Reference plant	IL 20%	IL 40%	IL 60%	IL 80%	Unit
Average clinker production		**118**	**118**	**118**	**118**	**118**	**t_{clk}/h**
Coal consumption		**15.28**	**12.67**	**10.45**	**8.34**	**6.23**	**t_f/h**
Pre-calciner		10.14	7.51	5.35	3.29	1.23	t_f/h
Rotatory kiln		5.14	5.16	5.10	5.05	4.99	t_f/h
Power consumption		**15.5**	**−7.9**	**−0.6**	**6.9**	**14.6**	**MW_{el}**
Clinker kiln auxiliaries		15.5	15.5	15.5	15.5	15.5	MW_{el}
CaL auxiliaries			6.0	5.7	5.4	5.2	MW_{el}
CO_2 compression			8.9	8.6	8.3	7.9	MW_{el}
Rankine cycle			−38.2	−30.4	−22.3	−14.0	MW_{el}
Solar calciner average heat consumption			**98**	**94**	**91**	**87**	**MW_{th}**
Solar calciner maximum heat consumption			401	385	369	353	MW_{th}
Heliostat field size	$S_{he,min}$		0.938	0.900	0.863	0.825	km^2
Cooling demand			**66.1**	**55.3**	**43.9**	**32.4**	**MW_{th}**
CO_2 compression			15.2	14.7	14.2	13.6	MW_{th}
Rankine cycle			50.9	40.5	29.7	18.8	MW_{th}
Total CO_2 emissions		**103.9**	**6.2**	**6.4**	**6.7**	**7.1**	**t_{CO2}/h**
Direct emissions		99.6	8.3	6.6	4.8	3.0	t_{CO2}/h
Indirect emissions		4.3	−2.2	−0.2	1.9	4.1	t_{CO2}/h
Captured CO_2			**87**	**84**	**81**	**78**	**t_{CO2}/h**
Total CO_2 produced			**95**	**90**	**86**	**81**	**t_{CO2}/h**
Specific primary energy consumption	**q_{clk}**	**4′488**	**5′535**	**5′312**	**5′137**	**4′973**	**MJ/t_{clk}**
Coal	$q_{fuel,clk}$	3′595	2′981	2′459	1′961	1′465	MJ/t_{clk}
Electricity	$q_{el,clk}$	894	−454	−37	400	843	MJ/t_{clk}
Thermal energy from solar	$q_{sol,clk}$		3′008	2′889	2′776	2′665	MJ/t_{clk}
Specific CO_2 emissions	**$e_{clk,eq}$**	**882**	**52**	**55**	**57**	**60**	**kg_{CO2}/t_{clk}**
Direct emissions	e_{clk}	846	71	56	41	26	kg_{CO2}/t_{clk}
Indirect emissions	$e_{el,clk}$	36	−19	−1	16	34	kg_{CO2}/t_{clk}
Carbonator average CaO conversion	**X_{ave}**		**27.7**	**46.5**	**61.8**	**71.8**	**%**
Specific CO_2 captured	**$m_{CO2,capt}$**		**738**	**713**	**686**	**659**	**kg_{CO2}/t_{clk}**
Specific CO_2 produced	**$m_{CO2,gen}$**	**846**	**808**	**769**	**727**	**685**	**kg_{CO2}/t_{clk}**
Carbon Capture Ratio	**CCR**		**91.2**	**92.7**	**94.4**	**96.2**	**%**
Equivalent Avoided CO_2	**AC_{eq}**		**94.1**	**93.8**	**93.5**	**93.2**	**%**
Avoided-Captured CO_2 Ratio	**ACR**		**1.13**	**1.16**	**1.20**	**1.25**	**-**
Specific Primary Energy Consumption for CO_2 Avoided	**SPECCA**		**1.26**	**0.99**	**0.79**	**0.59**	**MJ/kg_{CO2}**

the CaL. Estimated values of X_{ave} range from 27.7% at IL 20%–71.8% at IL 80% and are in agreement with experimental data reported in literature (Stendardo and Foscolo, 2009). For these reasons, low IL configurations present a reduced thermal energy consumption at the solar calciner. On the other hand, the amount of heat produced at the carbonator, and thus electricity produced in the Rankine Cycle, decreases with increasing IL values. In conclusion, systems with high integration levels seem to be more efficient from an energy point of view, having lower values of SPECCA and higher values of ACR. The reduction of the electricity production, however, results in overall higher indirect CO_2 emissions and, therefore, slightly lower values of AC_{eq}.

4.2. CaO solid storage size

Fig. 6 shows the reduction of the CaO storage size over increasing heliostat field area for different values of IL. Overall, the size of the storage is higher for lower IL indexes, and similar decreasing trend with increasing sf_{he} values was observed for all the IL values considered. The maximum value obtained, of around 550′000 t_{CaO} was found for IL = 20% and $sf_{he} = 1$, which can be reduced to 360′000 t_{CaO} increasing the value of sf_{he} to 7.5. However, for IL = 80% the estimated dimensions of the CaO solid storage are much smaller and range from 170′000 t_{CaO} ($sf_{he} = 1$) to 110′000 t_{CaO} ($sf_{he} = 7.5$). Configurations with higher IL seem, therefore, to be more advantageous also regarding land occupation, as they require smaller solid storages with similar heliostat field dimensions.

4.3. Electricity mix

Fig. 7 and Table 7 show the influence of the grid electricity mix on the main KPIs. In detail, Fig. 7 a shows the influence of the grid electricity mix and IL on the SPECCA index, while Fig. 7b and Fig. 7c shows the corresponding AC_{eq} and ACR values.

Moving from a higher carbon intensive electricity production to a less one, the reduction of the indirect emissions due to on-site power production from the Rankine cycle decreases, resulting in higher SPECCA and lower ACR values (Fig. 7a and Fig. 7c). For example, considering a 100% electricity production for renewable (Scenario 3), the SPECCA is around 2.17 MJ/kg_{CO2} for IL equal to 20%, while it decreases down to 0.62 MJ/kg_{CO2} for IL equal to 80%. For a higher carbon intensive electricity mix, lower SPECCA values and a lower variation over the IL are observed. In Scenario 1 (electricity production from coal) the SPECCA values varies from 0.84 MJ/kg_{CO2} at IL equal to 20% to 0.57 MJ/kg_{CO2} at IL equal to 80% (Fig. 7a).

Regarding the ratio between the avoided and captured CO_2 (ACR index) we obtained an increasing trend with the IL value for the reference scenario, scenario 2 and scenario 3. In scenario 3, for example, the ACR index increases from a minimum of 1.05 obtained at IL 20% to a value of 1.24 estimated at IL 80%. A different trend is obtained for scenario 1, where ACR varies slightly between 1.26 at IL equal to 20% and 1.25 at IL equal to 80% (Fig. 7c).

Fig. 7 b shows, instead, how the grid electricity mix influences the CO_2 emissions reduction. In detail, while for Scenario 3 the value of AC_{eq} increases from 91,6% (IL equal to 20%) to 97% (IL equal to 80%), an opposite trend is observed for all the other electricity mix considered. For example, in Scenario 1 a value of AC_{eq} of 97.9% is reached for IL equal to 20%, and an AC_{eq} value of 87.2% is obtained for IL equal to 80%.

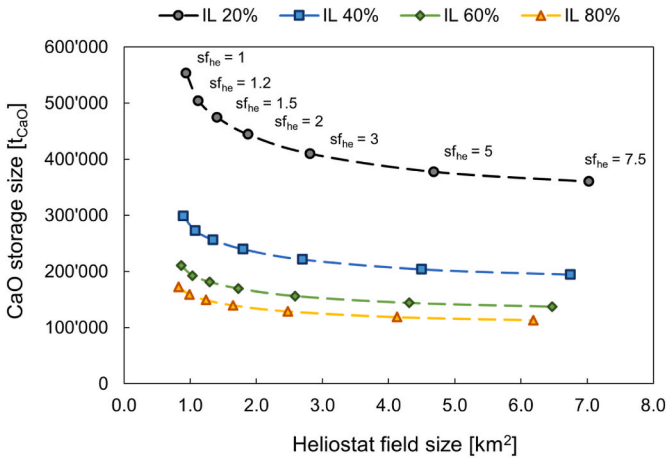

Fig. 6. Sensitivity of the CaO storage size with respect the heliostat field size.

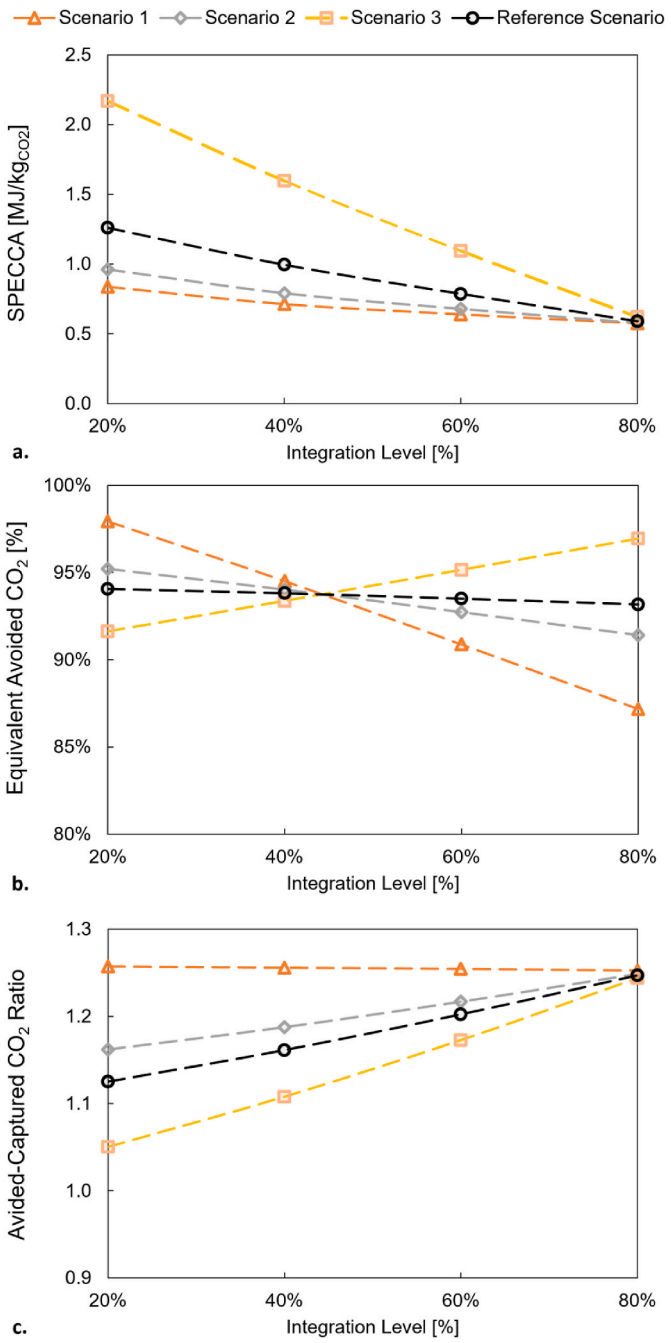

Fig. 7. Variation of the SPECCA, AC_{eq}, and ACR considering the different electricity mix and IL values (20–80%).

Table 7
Primary energy consumption, total CO_2 emissions and estimation of SPECCA, AC_{eq} and ACR for different electricity mixes.

Parameter	Symbol	Reference plant	IL 20%	IL 40%	IL 60%	IL 80%	Unit
Reference Scenario - Italian electricity mix							
Specific primary energy consumption	q_{clk}	4′488	5′535	5′312	5′137	4′973	MJ/t_{clk}
Specific CO_2 emissions	$e_{clk,eq}$	882	52	55	57	60	kg_{CO2}/t_{clk}
Specific Primary Energy Consumption for CO_2 Avoided	SPECCA		1.26	0.99	0.79	0.59	MJ/kg_{CO2}
Equivalent Avoided CO_2	AC_{eq}		94.1%	93.8%	93.5%	93.2%	%
Avoided-Captured CO_2 Ratio	ACR		1.13	1.16	1.20	1.25	–
Scenario 1 - State-of-the-art pulverized coal							
Specific primary energy consumption	q_{clk}	4′667	5′444	5′305	5′217	5′141	MJ/t_{clk}
Specific CO_2 emissions	$e_{clk,eq}$	947	19	52	86	121	kg_{CO2}/t_{clk}
Specific Primary Energy Consumption for CO_2 Avoided	SPECCA		0.84	0.71	0.64	0.57	MJ/kg_{CO2}
Equivalent Avoided CO_2	AC_{eq}		97.9%	94.5%	90.9%	87.2%	%
Avoided-Captured CO_2 Ratio	ACR		1.26	1.26	1.25	1.25	–
Scenario 2 – Italian traditional fossil power plants							
Specific primary energy consumption	q_{clk}	4′636	5′460	5′306	5′203	5′112	MJ/t_{clk}
Specific CO_2 emissions	$e_{clk,eq}$	900	43	54	65	77	kg_{CO2}/t_{clk}
Specific Primary Energy Consumption for CO_2 Avoided	SPECCA		0.96	0.79	0.68	0.58	MJ/kg_{CO2}
Equivalent Avoided CO_2	AC_{eq}		95.2%	94.0%	92.7%	91.4%	%
Avoided-Captured CO_2 Ratio	ACR		1.16	1.19	1.22	1.25	–
Scenario 3–100% Renewable energy sources							
Specific primary energy consumption	q_{clk}	4′068	5′748	5′329	4′949	4′577	MJ/t_{clk}
Specific CO_2 emissions	$e_{clk,eq}$	846	71	56	41	26	kg_{CO2}/t_{clk}
Specific Primary Energy Consumption for CO_2 Avoided	SPECCA		2.17	1.60	1.09	0.62	MJ/kg_{CO2}
Equivalent Avoided CO_2	AC_{eq}		91.6%	93.4%	95.2%	97.0%	%
Avoided-Captured CO_2 Ratio	ACR		1.05	1.11	1.17	1.24	–

5. Conclusions

In this work, the decarbonization of a cement plant was assessed by looking at the integration between CaL and CSP within the cement production process. We considered different levels of integration between the carbon capture system and the state-of-the-art clinker kiln and compared the energy and environmental performances of such system configurations. Results show a reduction of around 90%, or more, of the CO_2 emissions at the expense of an increased consumption of primary energy (+41%/+10% depending on the IL and grid electricity mix). The use of solar energy in the CaL, however, avoids the consumption of additional fossil fuel for the regeneration of the CO_2 sorbent. Furthermore, the reuse of the purged sorbent in the cement kiln reduces the energy required for limestone calcination in the clinker kiln, thus decreasing the overall coal consumption in the plant and the amount of CO_2 produced during the whole cement production process. For these reasons, the CO_2 emissions reduction is higher than the captured CO_2 (ACR >1), differently from typical CC-CaL systems (ACR <1). On the other hand, the integration of a solar-driven CaL system requires a large heliostat field (0.94–0.83 km^2 for a plant located in Sicily, Italy), to supply the amount of thermal energy needed for sorbent regeneration. It is also required the installation of components today still at a low TRL (4–5), such as: solar calciners, indirect gas-solid heat exchangers and solid-solid heat exchangers.

Thanks to the CaL carbonator's high operating temperatures, part of the energy supplied at the solar calciner can be recovered to produce electricity through a Rankine cycle. The power produced can be used in the cement plant reducing the electricity supplied from the grid, and, therefore, the indirect plant CO_2 emissions. For low IL, furthermore, the electricity produced is higher than the consumption and the surplus can be exported to the grid.

Furthermore, a sensitivity analysis was performed to investigate the size of the CaO storage at different values of sf_{he} and IL. Configurations with higher IL require much a smaller CaO storage: considering $sf_{he} = 1$, a storage dimension of around 170′000 t_{CaO} were obtained for IL = 80% against a value of 550′000 for IL = 20%. The storage size can then be further reduced by oversizing the heliostat field (increasing the sf_{he}). However, the optimal sizes of the solid storage and the solar field will need to be obtained through dedicated techno-economic analysis and should be investigated in future studies.

The evaluation of the main KPIs was performed considering different grid electricity mixes at different carbon intensities. When generation from pulverized coal or traditional fossil power plants with high CO_2 emission factors is assumed, on-site electricity production has a positive impact on the system's primary energy consumption and total CO_2 emissions. In these scenarios, configurations with low IL enable a deeper decarbonization of the process at the expense of higher SPECCA values. On the other hand, when 100% electricity production from renewable sources is considered, on-site production does not reduce the process indirect CO_2 emissions, resulting in overall higher SPECCA indexes. In this scenario configurations with high IL are preferred both in terms of energy consumption and CO_2 emissions.

Credit author statement

Daniele Ferrario: Conceptualization, Methodology, Writing – original draft preparation, Writing – review & editing. Andrea Lanzini: Methodology, Writing – original draft preparation, Writing – review & editing, Supervision, Funding acquisition. Stefano Stendardo: Methodology, Writing – original draft preparation, Writing – review & editing, Supervision, Funding acquisition. Vittorio Verda: Supervision, Funding acquisition.

Declaration of competing interest

The authors declare the following financial interests/personal relationships which may be considered as potential competing interests: Stefano Stendardo reports financial support was provided by Government of Italy Ministry of Sustainable Economic Development.

Data availability

Data will be made available on request.

Acknowledgements

The authors acknowledge the financial support received by the Italian Ministry of Sustainable Economic Development within the research programme 2019–2021: "Ricerca di Sistema" [Grant number: I34I19005780001].

Appendix A. Supplementary data

Supplementary data to this article can be found online at https://doi.org/10.1016/j.jclepro.2023.136367.

References

Abanades, J.C., Anthony, E.J., Wang, J., Oakey, J.E., 2005. Fluidized bed combustion systems integrating CO2 capture with CaO. Environ. Sci. Technol. 39 (8), 2861–2866. https://doi.org/10.1021/es0496221.

Arias, B., Alonso, M., Abanades, C., 2017. CO2 capture by calcium looping at relevant conditions for cement plants: experimental testing in a 30 kWth pilot plant. Ind. Eng. Chem. Res. 56 (10), 2634–2640. https://doi.org/10.1021/acs.iecr.6b04617. Mar.

Atsonios, K., Grammelis, P., Antiohos, S.K., Nikolopoulos, N., Kakaras, E., 2015. Integration of calcium looping technology in existing cement plant for CO2 capture: process modeling and technical considerations. Fuel 153, 210–223. https://doi.org/10.1016/j.fuel.2015.02.084.

Carbone, C., Ferrario, D., Lanzini, A., Stendardo, S., Agostini, A., 2022. Evaluating the carbon footprint of cement plants integrated with the calcium looping CO2 capture process. Front. Sustain. 3, 14. https://doi.org/10.3389/frsus.2022.809231.

CEMCAP, 2017. D3.2 CEMCAP framework for comparative techno-economic analysis of CO 2 capture from cement plants [Online]. Available: https://www.sintef.no/projectweb/cemcap/results/.

Chacartegui, R., Alovisio, A., Ortiz, C., Valverde, J.M., Verda, V., Becerra, J.A., 2016. Thermochemical energy storage of concentrated solar power by integration of the calcium looping process and a CO2 power cycle. Appl. Energy 173, 589–605. https://doi.org/10.1016/j.apenergy.2016.04.053.

Chang, M.H., et al., 2014. Design and experimental testing of a 1.9MWth calcium looping pilot plant. Energy Proc. 63, 2100–2108. https://doi.org/10.1016/j.egypro.2014.11.226.

Cormos, A.M., Cormos, C.C., 2017. Reducing the carbon footprint of cement industry by post-combustion CO2 capture: techno-economic and environmental assessment of a CCS project in Romania. Chem. Eng. Res. Des. 123, 230–239. https://doi.org/10.1016/j.cherd.2017.05.013.

De Lena, E., et al., 2017. Process integration study of tail-end Ca-Looping process for CO2 capture in cement plants. Int. J. Greenh. Gas Control 67 (October), 71–92. https://doi.org/10.1016/j.ijggc.2017.10.005.

De Lena, E., et al., 2019. Techno-economic analysis of calcium looping processes for low CO2 emission cement plants. Int. J. Greenh. Gas Control 82, 244–260. https://doi.org/10.1016/j.ijggc.2019.01.005. October 2018.

Enel, 2010. At Priolo Enel Inaugurates the 'Archimede' Power Plant, vol. 795.

EUROSTAT, 2022. Calculation methodologies for the share of renewables in energy consumption - statistics Explained. https://ec.europa.eu/eurostat/statistics-explained/index.php?title=Calculation_methodologies_for_the_share_of_renewables_in_energy_consumption.

Fennell, P.S., Davis, S.J., Mohammed, A., 2021. Decarbonizing cement production. Joule 5 (6), 1305–1311. https://doi.org/10.1016/j.joule.2021.04.011.

Fidaros, D., Baxevanou, C., Dritselis, C., Vlachos, N., 2007. Modelling of combustion and calcination in a cement precalciner, 2007 Proceedings of the European Combustion Meeting 1–6 [Online]. Available: https://www.researchgate.net/publication/237516535.

Gardarsdottir, S.O., et al., 2019. Comparison of technologies for CO 2 capture from cement production—Part 2: cost analysis. Energies 12 (3), 542. https://doi.org/10.3390/en12030542.

Gonzalez, R.S., Flamant, G., 2014. Technical and economic feasibility analysis of using concentrated solar thermal technology in the cement production process : hybrid approach — a case study. J. Sol. Energy Eng. 136 (May), 1–12. https://doi.org/10.1115/1.4026573.

Hills, T., Leeson, D., Florin, N., Fennell, P., 2016. Carbon capture in the cement industry: technologies, progress, and retrofitting. Environ. Sci. Technol. 50 (1), 368–377. https://doi.org/10.1021/acs.est.5b03508.

IEA, 2021. Cement. Paris, [Online]. Available: https://www.iea.org/reports/cement.

IEAGHG, 2015. Integrated carbon capture and storage project at saskpower' s boundary dam power station [Online]. Available: https://ieaghg.org/docs/General_Docs/Reports/2015-06.pdf.

ISPRA, 2020. Emission factors for electricity production and consumption in Italy - in Italian. http://www.sinanet.isprambiente.it/it/sia-ispra/serie-storiche-emissioni/fattori-di-emissione-per-la-produzione-ed-il-consumo-di-energia-elettrica-in-italia/view.

Jayarathna, C.K., Mathisen, A., Øi, L.E., Tokheim, L.A., 2017. Aspen Plus® process simulation of calcium looping with different indirect calciner heat transfer concepts. Energy Proc. 114 (1876), 201–210. https://doi.org/10.1016/j.egypro.2017.03.1162.

John, J.P., 2020. Parametric studies of cement production processes. J. Energy 1–17. https://doi.org/10.1155/2020/4289043, 2020.

Jordal, K., et al., 2017. Cemcap - making CO2 capture retrofittable to cement plants. Energy Proc. 114, 6175–6180. https://doi.org/10.1016/j.egypro.2017.03.1755.

Jordison, N., Rozendaal, N.A., Huang, P.X., 2007. Indirect-heat Thermal Processing of Particulate Material. US 8578624 B2.

Khosravi, S., Hossainpour, S., Farajollahi, H., Abolzadeh, N., 2022. Integration of a coal fired power plant with calcium looping CO2 capture and concentrated solar power generation: energy, exergy and economic analysis. Energy 240, 122466. https://doi.org/10.1016/j.energy.2021.122466.

Liu, M., et al., 2016. Review on concentrating solar power plants and new developments in high temperature thermal energy storage technologies. Renew. Sustain. Energy Rev. 53, 1411–1432. https://doi.org/10.1016/j.rser.2015.09.026. Pergamon.

Merchán, R.P., Santos, M.J., Medina, A., Calvo Hernández, A., 2022. High temperature central tower plants for concentrated solar power: 2021 overview. Renew. Sustain. Energy Rev. 155, 111828. https://doi.org/10.1016/J.RSER.2021.111828.

Moumin, G., et al., 2020. CO2 emission reduction in the cement industry by using a solar calciner. Renew. Energy 145, 1578–1596. https://doi.org/10.1016/j.renene.2019.07.045.

Ortiz, C., Chacartegui, R., Valverde, J.M., Alovisio, A., Becerra, J.A., 2017. Power cycles integration in concentrated solar power plants with energy storage based on calcium looping. Energy Convers. Manag. 149, 815–829. https://doi.org/10.1016/j.enconman.2017.03.029.

Ortiz, C., Romano, M.C., Valverde, J.M., Binotti, M., Chacartegui, R., 2018. Process integration of Calcium-Looping thermochemical energy storage system in concentrating solar power plants. Energy 155, 535–551. https://doi.org/10.1016/j.energy.2018.04.180.

Ortiz, C., Valverde, J.M., Chacartegui, R., Perez-Maqueda, L.A., Giménez, P., 2019. The Calcium-Looping (CaCO3/CaO) process for thermochemical energy storage in Concentrating Solar Power plants. Renew. Sustain. Energy Rev. 113, 109252 https://doi.org/10.1016/j.rser.2019.109252. June.

Ortiz, C., Valverde, J.M., Chacartegui, R., Pérez-Maqueda, L.A., Gimenez-Gavarrell, P., 2021. Scaling-up the calcium-looping process for co2 capture and energy storage. KONA Powder Part. J. 38, 189–208. https://doi.org/10.14356/kona.2021005.

Plaza, M.G., Martínez, S., Rubiera, F., 2020. CO2 capture, use, and storage in the cement industry: state of the art and expectations. Energies 13 (21), 5692. https://doi.org/10.3390/en13215692.

Posch, S., Haider, M., 2012. Optimization of CO 2 compression and purification units (CO 2CPU) for CCS power plants. Fuel 101, 254–263. https://doi.org/10.1016/j.fuel.2011.07.039.

PVGIS, 2019. JRC Photovoltaic Geographical Information System (PVGIS) - European Commission. *Photovoltaic Geographical Information System*. https://re.jrc.ec.europa.eu/pvg_tools/en/.

Schorcht, F., Kourti, I., Scalet, B.M., Roudier, S., Sancho, L.D., 2013. Best Available Techniques (BAT) Reference Document for the Production of Cement, Lime and Magnesium Oxide. European Commission Joint Research Centre [Online]. Available: https://eippcb.jrc.ec.europa.eu/sites/default/files/2019-11/CLM_Published_def_0.pdf.

Stendardo, S., Foscolo, P.U., 2009. Carbon dioxide capture with dolomite: a model for gas-solid reaction within the grains of a particulate sorbent. Chem. Eng. Sci. 64 (10), 2343–2352. https://doi.org/10.1016/j.ces.2009.02.009.

Tesio, U., Guelpa, E., Verda, V., 2020. Integration of thermochemical energy storage in concentrated solar power. Part 1: energy and economic analysis/optimization. Energy Convers. Manag. X 6, 100039. https://doi.org/10.1016/j.ecmx.2020.100039. March.

Wu, W., Trebing, D., Amsbeck, L., Buck, R., Pitz-Paal, R., 2015. Prototype testing of a centrifugal particle receiver for high-temperature concentrating solar applications. J. Sol. Energy Eng. Trans. ASME 137 (4). https://doi.org/10.1115/1.4030657.

Zhai, R., Li, C., Qi, J., Yang, Y., 2016. Thermodynamic analysis of CO2 capture by calcium looping process driven by coal and concentrated solar power. Energy Convers. Manag. 117, 251–263. https://doi.org/10.1016/j.enconman.2016.03.022.

Zhang, X., Liu, Y., 2014. Performance assessment of CO2 capture with calcination carbonation reaction process driven by coal and concentrated solar power. Appl. Therm. Eng. 70 (1), 13–24. https://doi.org/10.1016/j.applthermaleng.2014.04.072.

Zsembinszki, G., Sole, A., Barreneche, C., Prieto, C., Fernández, A.I., Cabeza, L.F., 2018. Review of reactors with potential use in thermochemical energy storage in concentrated solar power plants. Energies 11 (9), 2358. https://doi.org/10.3390/en11092358.